Thermal and hydraulic behaviors of a finned coil heat exchanger coupled with fixed-speed fans during frost formation in an industrial food freezer: numerical modelling and field experimental validation

Deyae Badri, Cyril Toublanc, Michel Havet, Olivier Rouaud

DOI: 10.18462/iir. 10.18462/iir.icr.2023.0605

Thermal and hydraulic behaviors of a finned coil heat exchanger coupled with fixed-speed fans during frost formation in an industrial food freezer: numerical modelling and field experimental validation

Deyae BADRI [a], Cyril TOUBLANC*[a], Olivier ROUAUD[a], Michel HAVET[a]

(a) Oniris, Nantes Université, CNRS, GEPEA, UMR 6144, F-44000, Nantes, France,

*cyril.toublanc@oniris-nantes.fr

ABSTRACT

Frost management is a major concern for frozen food industry manufacturer with significant economic consequences. The present paper describes numerical and experimental approaches analysing the transient heat transfer and flow phenomena of a freezing equipment operating under frosting conditions. The frost model developed considers the temporal phenomena of thickening and densification of the frost layer. The frost model was compared to experimental data from the literature before being integrated in the finned tube heat exchanger model coupled with a fixed-speed axial fan. The whole model results were then compared with field measurements carried out on a real production line. Experimental devices have been deployed to monitor the reduction of the airflow cross-section through the exchanger as well as the reduction of the convective heat transfer coefficient on the conveyor belt on which the products are positioned.

Keywords: spiral-freezer, frost, numerical modelling, evaporator, food freezing.

1. INTRODUCTION

Freezing is regarded as one of the best methods for long-term food preservation as chemical reactions and microbial growth are reduced at low temperatures. Blast freezing is the process of pushing the air cooled by the evaporators (around -40 °C) at high velocity (>3 m/s), using fans, across a food product in order to freeze the product as fast as possible.

When the moisture in the air encounters a surface with a temperature below 0 °C, frost formation occurs. In industrial freezing where temperatures are very low, frost formation is therefore almost inevitable. When accumulated on the surface of the heat exchanger, it leads to a decrease of its thermal performance which, after a period of time and if no corrective action is taken, leads to non-conforming food products at the freezer outlet due to a too low degree of freezing. To overcome practically this problem, it is possible to extend the residence time of the products within the equipment but this solution can only be temporary and it is then imperative to defrost the finned coil heat exchanger. The solution would be to have a dimensioning and a controlling of the freezers adapted to the treated products and to the industrial practices. To do this, it is important to understand how, during a production session, the heat transfer resistance and the airflow resistance evolve.

Several studies have been carried out to investigate the frosting/defrosting process in different conditions and for different geometries. Many researchers have investigated the frosting phenomenon by focusing on the evaporator since it is the critical component. In addition, most of these researches have been performed under air-conditioning conditions (Léoni et al. 2016). For deep freezing conditions (low temperature and high air relative humidity), the available literature is more limited (Aljuwayhel et al. 2008). This paper aims to bridge the gap of the literature by investigating with both numerical and experimental approaches the thermal and hydraulic behavior of a finned tube heat exchanger during frost formation.

2. EXPERIMENTAL AND NUMERICAL STUDY

The freezer, which is the main object of the present study, is a spiral air blast freezer operating with an ammonia overfeed finned tube evaporator and having a cooling capacity of about 126 kW. It is a real system of an agrifood French company that produces frozen pizzas and which regularly faces to non-conform food products due to frost accumulation on the evaporator.

The 2-pass spiral air-blast freezer, depicted in **Figure 1**, comprises a set of 24 spirals, resulting in a cumulative belt length of 370 meters. The evaporator employed in this system is a finned and tube heat exchanger, through which cold air is circulated by an axial fan, ensuring uniform airflow distribution across the entire width of the freezer.

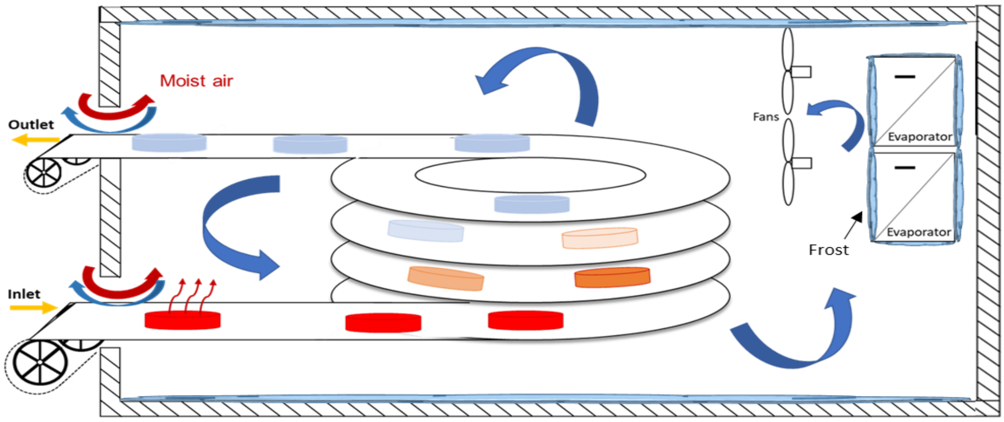

Figure 1: Schematic of the studied spiral air blast freezer under frosting conditions.

This installation should run during a full production day, i.e., at least more than 15 hours without any significant decrease of the refrigerating capacity. Indeed, a single defrosting sequence is daily launched outside production hours during the night. Unfortunately, it happens that after only few hours of production, the staff notices that the products are inadequately frozen upon existing the freezer. In this circumstance, they have to increase the residence time of products within the freezer by reducing the speed of the conveyor belt, which, in turn, decreased the production rate. Occasionally, this adjustment only served as a temporary solution, necessitating a complete halt in production to manually remove frost from the evaporator using a scrubbing brush. Such a situation was encountered during the test campaign. That day the manufacturer was producing large unpackaged rectangular pizzas. Each was measuring l: 510 × w: 310 x h: 10 mm and had a residence time of about 42 minutes. The frozen pizzas have around 1.6 kg as unitary mass. **Table 1** summarizes all the system data and operating conditions. Thereafter, the experimental campaign will be described and the numerical model will be presented.

Table 1: Freezing system data and operating conditions.

Evaporator type	Finned tube
Evaporator coil feeding type	Controlled pressure receiver liquid overfeeds
Evaporator circuiting type	Parallel
Evaporator fin pitch	Progressive fin pitch 24/12/8 mm
Nominal capacity	126 kW
Refrigerant	Ammonia
Evaporation Temperature	-40 °C
Evaporator air inlet temperature (nominal)	-35 °C
Number of fans	1
Nominal airflow rate	76,000 m^3/h
Nominal air velocity at the front area	4.32 m/s
Vapor-Liquid separator capacity (Low pressure)	6 m^3
Vapor-Liquid separator capacity (Medium pressure)	3 m^3
Condenser water cooler system	Cooling tower

2.1. Material and Methods

An experimental investigation has been conducted by GEPEA laboratory, CETIAT industrial technical center and GEA Refrigeration company. The objective of this study was to determine the nominal operational conditions, which were subsequently used to initialize and configurate the numerical model. The second objective was to examine the freezing system behaviour during a typical production day in a frozen food manufacturing facility.

2.1.1. Air pressure and velocity measurements

Pitot tubes were placed downstream and upstream of the evaporator and the fan in order to measure the static and total pressures. These measurements were carried out in nominal conditions first (freezing system being turned off), in order to determine the nominal heat exchanger pressure-drop, the frontal air velocity and the fan nominal pressure and airflow rate. Thereafter, the same measurements were made under frost conditions in order to dynamically monitor the influence of frost.

The static and total pressure were measured with a Pitot tube (KIMO 0 - 1,000 Pa ±3 Pa). By considering the evaporator frontal area, the air velocity was deduced.

The Pitot tubes were placed downstream and upstream of the evaporator and the fan. The cold coil has been divided into several meshes where the pressure sensors have been placed. It has been observed that the air velocity was uneven over the entire coil. This was due to the non-uniform ventilation and air distribution. For this reason, the air velocity values in each cell were recorded, and then averaged over the entire coil surface.

Under dry conditions, the velocity was not homogeneous on the whole surface, it oscillated between 3.57 and 5.14 m/s. The calculated average velocity being 4.32 m/s, the resulting volume airflow rate was approximately 76,000 m^3/h. The nominal fan static pressure was 231 Pa. According to the characteristic curve of the fan, this gives almost the same flow to that measured.

2.1.2. Frost growth and cross section area restriction

A recording camera was placed below the evaporator (at the inlet airside) (**Figure 2**) to monitor its front side. Also, it took pictures every 7 seconds. The camera, specifically a GO5000 model, is equipped with a sensor (2,560 × 2,048 pixels) associated with a RICOH FL-BC2518-9M lens with a focal length of 25 mm. The lens was positioned 60 cm from the ground, which means that the camera-object distance was 103 cm. Under these conditions, the observation area window was 0.22 m² (529 mm × 423 mm) which represented around 2.2 % of the total frontal section. The resolution of the image is 207 µm / pixel.

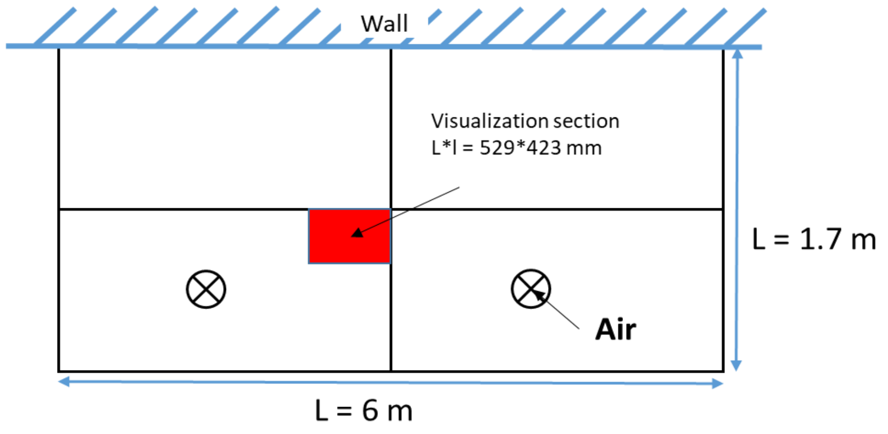

Figure 2: Location of the recording camera in front of the evaporator.

The camera was turned on during the cooling start-up period, just before food production. A recorded film was made at the rate of one image every 7 seconds. Several disturbances are visible in the film, slight movements of the camera, sudden change in brightness due to door opening or staff intervention, etc. From this film, 487 images were extracted with a time step of 112 s. As shown on **Figure 3**, the histograms of the images were normalized, using ImageJ software, to smooth out differences in illumination. In the CTAn software, the images were filtered in order to increase the local contrasts with a conditional mean filter (in 2D, round kernel of radius 3, threshold 50).

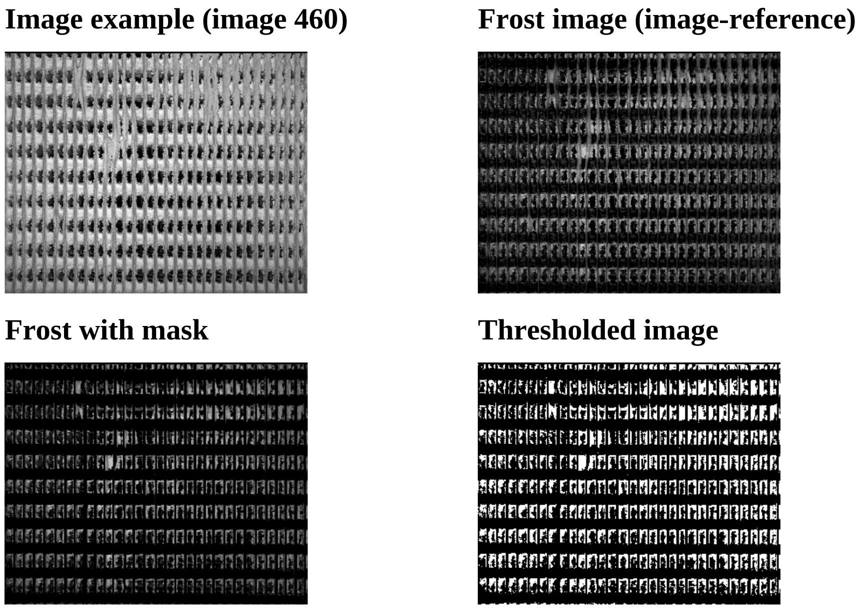

Figure 3: Example of image processing.

In ImageJ, the images have been aligned on the initial image (Stack Reg function) and a film has been made. An early image of the film was chosen to create the initial mask that offers a good contrast between the background and the coil. The mask was made from an overlay for the vertical tubes followed by thresholding. Then, this initial reference image was subtracted from all the following images, resulting in a film that exclusively captured the formation of frost during the recording. Finally, the mask was applied to these images, subjected to thresholding (gray level 44) to enhance the visibility of the formation in the free section of the coil. By employing this method, the area of the openings could be accurately calculated.

2.1.3. Air-product heat exchange quality

For the convective heat transfer coefficient of the food freezing process, a large number of convective heat transfer coefficient correlations have been obtained on the basis of experimental research, which can be directly used to calculate the convective heat transfer coefficient between food and air. However, these correlations are usually restricted to specific application conditions. For specific geometries and flow field in industrial process, it is often complex to adopt these heat transfer coefficient correlations. Thereby, a specific correlation was developed for the actual conditions.
The air-product convective heat transfer coefficient was measured by a specific heat flux sensors (**Figure 4**) placed, at different moments during the production day over 15 hours, on the conveyor at the freezer inlet. The sensor spent, as the product, 42 minutes before being picked up. The results were used in order to bring out an average air-product convective heat transfer coefficient for each passage. Two thermocouples were integrated into the experimental setup. One thermocouple was used to measure the air temperature while the second one was placed within the heat flux cell to monitor its temperature throughout the 42 minutes residence time.

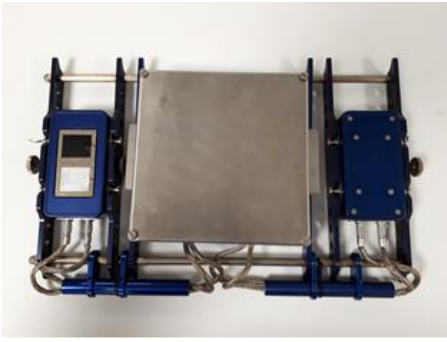

Figure 4: Airflow device for convective heat transfer coefficient measurement on conveyor (TPVOYAGER-CVT500).

Figure 5 illustrates the first recording measurement of the convective heat transfer coefficient (freezer empty) as function of the position on the conveyor belt. The position is defined depending on the full conveyor belt length L_0. It could be observed that the heat transfer coefficient oscillates depending on the horizontal distance from the fan. It is maximum when the products are on the fan side and minimum when they are on the opposite side. As consequence, for simplification reason, the convective heat transfer coefficient was averaged.

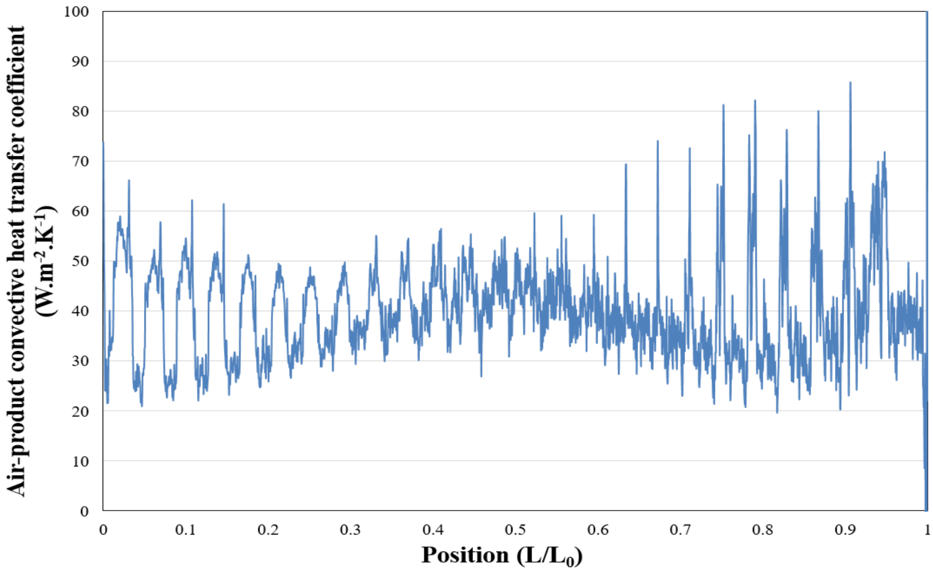

Figure 5: First air-product convective heat transfer coefficient measurements as function of the position on the conveyor belt.

At each moment, the corresponding air velocity was defined by experimental results in order to perform the following empirical correlation:

$$\alpha_p = 22.3 \times V_a^{0.4} \qquad \text{(Eq. 1)}$$

This correlation is valid for an apparent air velocity ranging from 2.5 m/s and 4.5 m/s.

2.1.4. Product water losses during freezing

The frost deposited on the exchanger is influenced by the relative humidity inside the freezer, which in turn depends on the water released by the products during their freezing process. Successive weight measurements of many products throughout the production day were done. A sampling of three products every half-hour (around one sample every 30 minutes) was performed. The weight of the same products was measured successively at the inlet and the outlet of the tunnel. As depicted in **Table 2** the rate of water loss during the freezing process for both pizza types represent almost 1.1% of the initial pizza weight. This value is in agreement with typical blast freezer application (Rouaud and Pham 2012).

Table 2: Experimental results of the amount of food water losses during freezing.

Pizza (1.6 kg each)	Water losses during freezing
Average losses (g)	16.8
Standard deviation (g)	2.2

2.2. Numerical study

The frost process and the overall system is modelled in Modelica, an equation-based, object-oriented modelling language (Fritzson 2012). The model equations are directly implemented and solved in Dymola environment version 2020x. In this paper, the components' models are adapted from *TIL* (Richter and Braunschweig n.d.) and *Building* libraries (Wetter et al. 2014) coupled with self-developed models. The numerical model architecture is presented in the **Figure 6**.

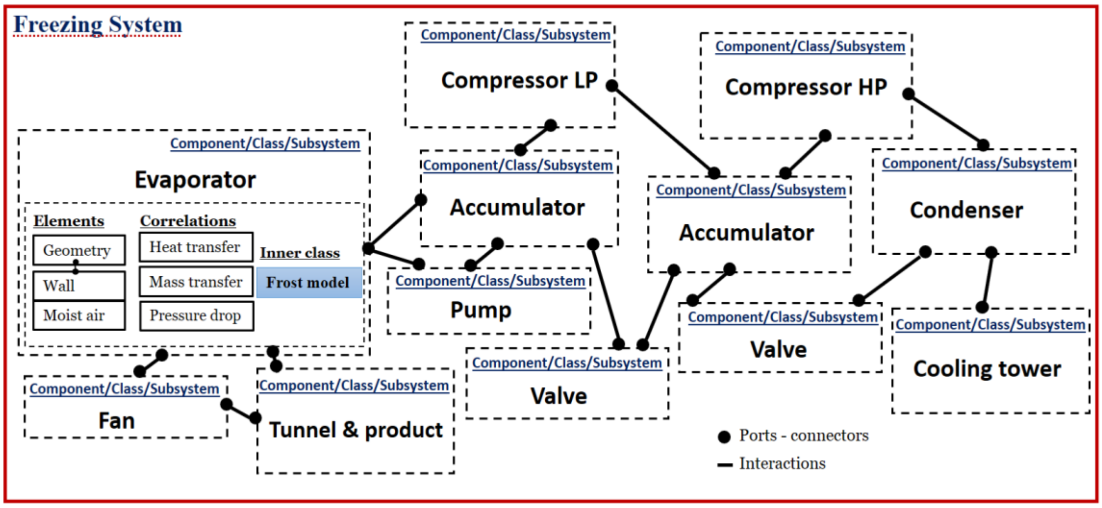

Figure 6: Freezing system modeling architecture.

2.2.1. Evaporator and condenser models

The evaporator and condenser models were chosen from the *heat exchangers* package of *TIL* library. The models are generally composed using cells (finite volume elements) to represent the two fluid flows and the separating wall resulting in a sandwich structure. A record geometry is adapted in order to describe the actual geometric parameters and material types. Then, internal functions compute the external and internal surfaces as well as the external and internal cross-sectional areas. These outputs are transmitted to the air, wall and fluid elements in order to solve heat transfer, mass transfer, pressure drop, and fin efficiency correlations.

For the refrigerant side, a constant heat transfer coefficient of 2,000 $W.m^{-2}.K^{-1}$ is assumed for the evaporator while the internal heat transfer coefficient is calculated using the correlation provided by Shah and London (Shah and London 1978). For airside, we have selected the heat transfer and pressure drop correlations based on the work of von Haaf (Haaf 1988) that were also used by Tegethoff (Tegethoff 1999) and Schmidt (Schmidt 2003).

The variation of both cross section and heat transfer area due to frost accumulation is taken into consideration using the void ratio and the similarity theorem of triangles, as suggested by Westhäuser et al. (2018).

2.2.2. Frost model

Since the present study focuses on an overall refrigeration system-level simulation, the aim was to develop a suitable frost model that takes as much as possible the physical phenomena but without any secondary details and computational complexity. The literature review showed that the only available empirical correlation able to predict frost properties under freezing conditions is not suitable to finned tube geometry (Mao, Chen, and Besant 1999). Moreover, the CFD based models seemed to be inconvenient with this type of industrial application (Kim, Kim, and Lee 2015). Therefore, a quasi-steady state modeling of frost accumulation is adopted, considering the frost layer as a one-dimension porous medium subject to heat (Eq.2) and mass transfer (Eq.3).

$$\dot{Q}_s'' = \alpha_a \times (T_{a,in} - T_\delta) \qquad \textbf{(Eq. 2)}$$

$$\dot{m}_v'' = \bar{\rho}_{fr} \frac{d\delta_{fr}}{dt} + \delta_{fr} \frac{d\bar{\rho}_{fr}}{dt} \qquad \textbf{(Eq. 3)}$$

Where T_δ is the frost surface temperature, α_a is the convective heat transfer coefficient. ρ_{fr} is the local density of the frost layer, $\bar{\rho}_{fr}$ and δ_{fr} are the average density and thickness of the frost layer, respectively. $\bar{\rho}_{fr} \frac{d\delta_{fr}}{dt} = \dot{m}_\delta''$ is the densification rate and $\delta_{fr} \frac{d\bar{\rho}_{fr}}{dt} = \dot{m}_\rho''$ is the thickening or the growth rate. The main goal of this physical model is to define each quantity of $\dot{m}_\delta''$ and $\dot{m}_\rho''$. For this purpose, the balance equations are divided in several parts ranging from the frost-air interface and cascading down to the cold plate at x=0 (Qiao and Radermacher 2014).

2.2.3. Separator model

The separators models were chosen from the TIL library Accumulator package. Their dynamic model is described by Strupp et al. (2007) and Bockholt et al. (2008).

2.2.4. Expansion valve model

The expansion valves models were selected from *Valves* package. Orifice valve model based on expansion coefficient is adopted. The model calculates the mass flow rate in function of the pressure drop using Bernoulli's equation. The mass flow rate could be computed by the equation below:

$$\dot{m}_v = A_{eff} \cdot \sqrt{(p_1 - p_2).2\rho_1} \qquad \textbf{(Eq. 4)}$$

where A_{eff} is the effective flow area, ρ_1 is the inlet refrigerant density, p_1 and p_2 are the inlet and outlet pressures, respectively. The effective flow area of the high-pressure side expansion valve is fixed at 4×10^{-6} m^2. For the low-pressure side, the effective flow area is variable in order to maintain a fixed pressure in the low-pressure tank.

2.2.5. Fan model

The fan model was selected from *Fans* package. A second order fan defined by quadratic characteristics and consideration of power losses is coupled to the evaporator. In our case, the fan used is the Woods® axial fan 48J ½, made with an 20° pitch angle, turning at a fixed 50 Hz frequency and has a maximal fin efficiency of 82%.

2.2.6. Medium

In the present model, gas, liquid, two-phase fluid and heat ports are used in order to transmit pressure, enthalpy, mass flow rate and heat flux.

Based on VDI heat atlas database (VDI Heat Atlas 2010) the moist air properties are calculated while the ammonia properties are based on Refprop 10.0 (Lemmon et al. 2021). These two media are defined in a component called SIM (system information manager) that stores all information related to their properties and also computes numerical information like the total refrigerant mass and total inner volume which are important system parameters.

2.2.7. Cooling tower

A model of a cooling tower with a water pump, featuring an ideally controlled mass flow rate as input signal is selected from *Building* library. This cooling tower is based on Approach temperature defined as the difference between the cold water temperature leaving the tower and the ambient wet bulb temperatures. This model is chosen in order to simplify the freezing system model since the cooling tower is considered for second interest in the whole analysis.

2.2.8. Screw Compressor

For this industrial ammonia systems, the compressor type used is a screw compressor with a fixed speed and variable capacity. The capacity is regulated using a slide valve. When the slide valve is opened, a portion of the gas inside the compressor is vented back to the suction port. This provides regulation down to 10% of full capacity. This type of regulation is easy but it affects the compressor efficiency.
To model this type of compressor, a model inspired from Liu et al. (Liu et al. 2012) is developed. It consists of predicting the compressor volumetric efficiency as function of pressure ratio and other variables detailed in equation (Eq.5).

$$\boldsymbol{\eta_v = a\tau^{\frac{1}{k}}\tau^{-1} + (b + c\tau^{-1})\tau^{\frac{1}{2k}}\sqrt{2v_1(p_2 - p_1)}} \qquad \text{(Eq.5)}$$

where, τ is the ratio of the discharging pressure and the suction pressure, *k* is the polytropic index, and a b and c are coefficients obtained through constructor data regression.

Since the relation between the slide position and the swept volume is not linear, a correcting factor is used to predict the volumetric efficiency for part-load conditions. Therefore, the volumetric efficiency can be calculated with equation (Eq.6).

$$\boldsymbol{\eta_v = \eta_{v\ 100\%} f(S_{vp})} \qquad \text{(Eq.6)}$$

where, $\eta_{v\ 100\%}$ is the full load volumetric efficiency, $f(S_{vp})$ is a correcting polynomial of degree 5 expressed as function of valve slide position. It is determined to fit with measured data. Doing this, the sucked vapor mass flow rate and the power transferred to the ammonia are deduced.

2.2.9. Internal freezer space and product

The interior freezer space including tunnel and products is modelled by an air volume with a heat flow source and a humidifier. The heat flow source represents the head load of the products to be frozen, thermal loads of air infiltrations, wall thermal losses, the conveyor belt heat load, and heat exchange between the tunnel and duct area. The humidifier modelled by a water vapor source represents water losses of the product during freezing. In addition, a hydraulic resistor is added to the air loop in order to take into consideration the pressure drop inside the freezer tunnel (**Figure 7**).

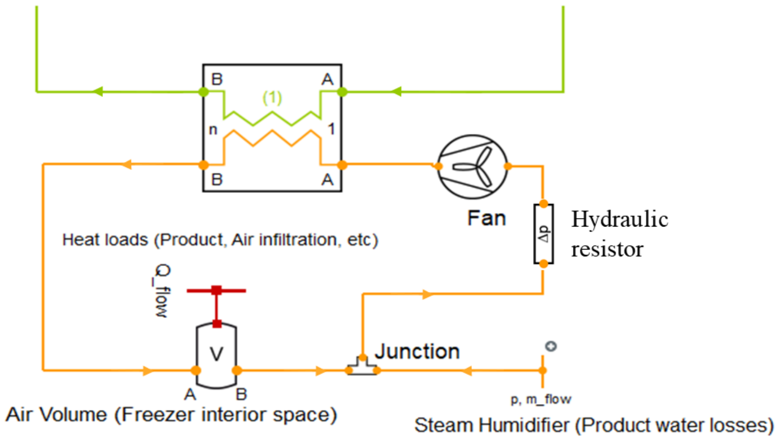

Figure 7: Air loop model on Dymola layout.

2.2.10. <u>Control</u>

All the system control is carried out by PID controllers. The latter are used to:

- Control the driver position of the compressors in order to maintain constant the pressures at the Vapor-Liquid separators (Low and medium pressures). The minimum driver position is limited to 40%;
- Control the valve section in order to maintain constant the filing level of the vapor liquid separator of medium pressure;
- Control the water flow rate of condenser pump in order to maintain constant the condensation pressure;
- Control the cooling tower fan speed in order to maintain constant the water exit temperature at the set point.

2.3. Results and discussions

As can be seen on **Figure 8**, the pressure drop across the evaporator continues to increase during the production cycle.

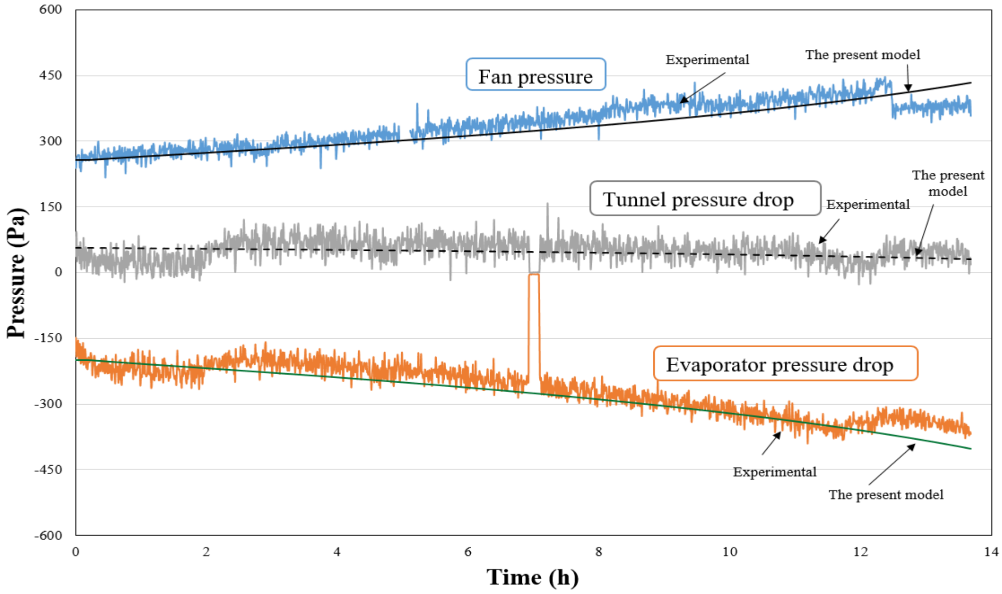

Figure 8: Experimental and numerical results: Fan pressure, pressure drop through the evaporator coil and tunnel.

The initial value is approximately 220 Pa, which corresponds to the experimental measurement and manufacturer's documentation at the nominal operating conditions. Operating under frosting conditions, the pressure drop increases to reach approximately 400 Pa, that means an increase of 100% compared to the initial value. This increase is due to the accumulation of frost on the coil, which ultimately has the effect of reducing the airflow through the coil. Note that the pressure supplied by the fan is the reverse image of the pressure drop: the fan undergoes pressure changes. The residual static pressure, determined through experimental measurements, is represented by the grey curve and is assumed to represent the pressure drop across the tunnel. The formation and accumulation of frost on the heat exchanger surface leads to a smaller airflow passage area. This has a direct impact on airside conditions by increasing the pressure drop across the coil. The experimental data indicates that the pressure drop progressively increases from 220 Pa to around 450 Pa by the end of the experiment. The actual model exhibits a similar trend. Numerical values are within 5% far from the experimental results.

By the end of production cycle, an intervention was made in order to scrape the front of the evaporator coil from frost. This operation proved to be effective, as evidenced by the slight reduction in pressure drop observed in the experimental curve. By the end, the pressure drop was around 380 Pa. This intervention could explain the discrepancy between numerical and experimental results by the end of the day.

One can observe from **Figure 9** that the air cross section area was reduced by almost 60% during the day.

The numerical model accurately predicts a similar trend during 15 hours. The difference between the numerical and experimental results could be attributed to multiple factors. The primary factor is the limited section captured by the camera which constitue only 2.2 % of the entire air passage section. considering that the frost is not distributed uniformly on the front face, this opening rate may not represent the average opening rate of the entire cold coil. Additionally, minor discrepancies could arise from measurement uncertainties.

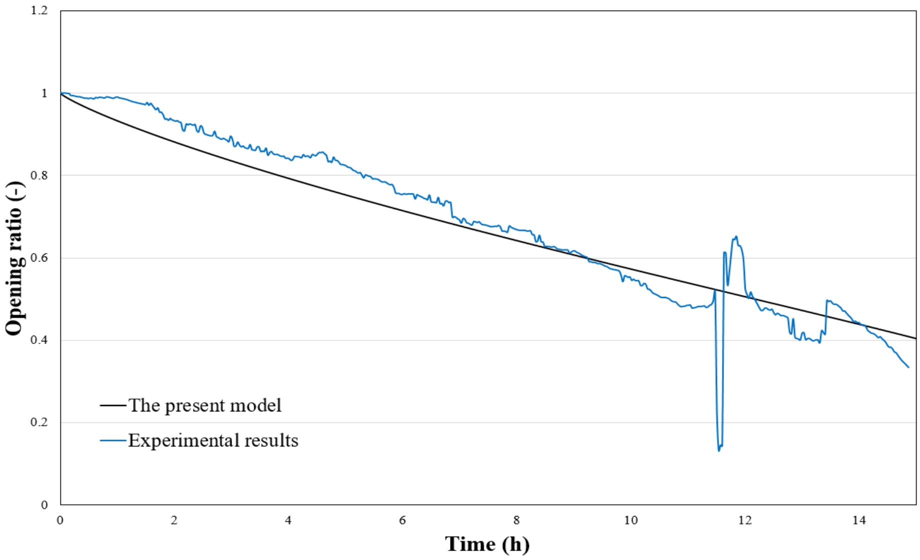

Figure 9: Experimental and numerical results of the cross-section area opening ratio.

Another phenomenon directly related to the blockage of the airflow passage section is the reduction of the Air-product heat transfer coefficient. According to **Figure 10**, the convective heat transfer coefficient decreases slowly at beginning of the freezing process then it increases slightly at the 12th hour of the production day. This could be attributed to the change of product after a freezing stop of one hour. Since the freezer was empty for an hour, the performance was slightly improved and the convective heat transfer coefficient at the introduction of the second product reached approximately 38 W.m^{-2}.K^{-1} compared to the end of the first production where it was around 36 W.m^{-2}.K^{-1}. This operation could also explain the slight difference between numerical and experimental results.

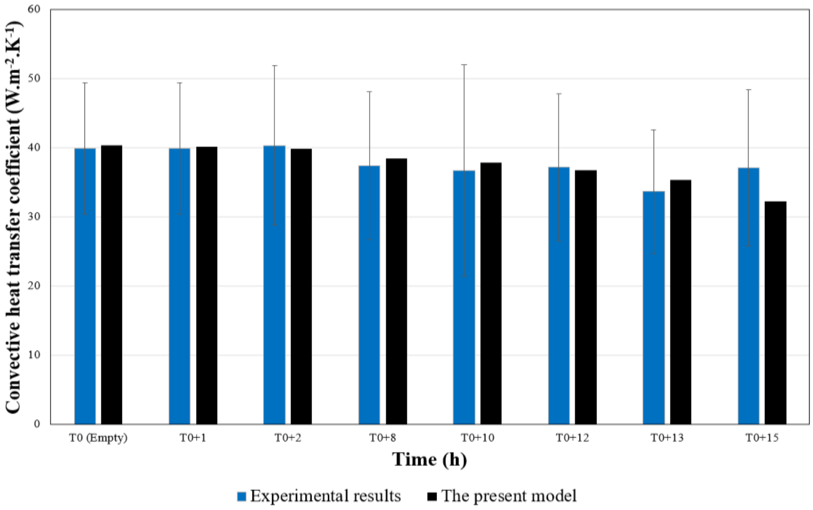

Figure 10: Experimental and numerical results: air-product convective heat transfer coefficient.

The interpretation of the whole situation could be that the reduction is directly attributed to the blockage of airflow passage due to the frost build-up. Taking into consideration the hydraulic coupling between the fan and the coil, the airflow reduces in fan-supplied evaporator which is one of the main causes of the heat exchange reduction. The cross-section area has been blocked by 80%, the pressure drops increases by 100%, and the heat transfer coefficient decreases by about 20%. It is to note that the standard deviation does not reflect the measurement uncertainty but rather the deviation of the convective coefficient values that varies as the heat flux device passes through the tunnel.

It is worth noting that this older type of installation may not fall within the realm of new blast freezer technologies, which are specifically designed for managing a specific high product moisture. Furthermore, it is used for freezing food products (Pizzas) directly from the oven, with a tomato sauce at a temperature of 40 °C. This could explain the significant degradation of performances, as observed both experimentally and numerically.

Indeed, resizing and designing the evaporator geometry to ensure the longest possible operating time before defrosting is a crucial step in addressing this phenomenon. However, it does not negate the fact that controlling product moisture loss is essential in industrial freezers. The difference in water vapor pressure between the food surface and the surrounding atmosphere (air freezer) drives dehydration, and this effect is more pronounced when the product is initially at a higher temperature (40 °C). Precooling the product before introducing it into the freezer can also be one of the recommended solutions ((Badri et al. 2021)).

3. CONCLUSIONS

A theoretical model of a whole and complete freezing system subjected to frost accumulation has been developed based on Modelica oriented object language. The model prediction agreed well with their experimental data in terms of air pressure drop, blockage ratio of the evaporator cross section area and the air-product convective heat transfer coefficient. As frost build-up, the free cross section area decreases resulting in an increase of pressure drops and a decrease of the air volume flow rate supplied by the fan. Moreover, the low thermal conductivity of the frost layer adds an additional thermal resistance between the air and the refrigerant. This degradation is clearly noticed in the heat exchange quality between air and the product. The comparisons between the simulation and experimental data show that the proposed model can be used to better understand the heat transfer and flow transient characteristics of the freezing system under real frosting conditions in order to optimize the design of the equipment. Further numerical results and analysis could be exploited to obtain possible data about the local aspect of frost on the evaporator as well as the effect of the frost accumulation on the energy performance and on the quality of the product during a typical industrial production day.

ACKNOWLEDGEMENTS

This work was supported by the French Agency for Ecological Transition through the FOODEFREEZE project (Grant n°1881C0024). The authors thank the partners CETIAT and GEA who carried out the measurements of pressures and airflow. They also thank Luc Guihard and Sylvie Chevallier for their help in performing experiments and image analysis, respectively.

NOMENCLATURE

A	area (m²)	T	temperature (K)
$\dot{m}$	mass flow rate ($kg.s^{-1}$)	V	velocity (m/s)
$\dot{m}''$	mass flux ($kg.s^{-1}.m^{-2}$)	α	convective heat transfer coefficient ($W.m^{-2}.K^{-1}$)
p	pressure (kPa)	η	efficiency

REFERENCES

Aljuwayhel, N.F., D.T. Reindl, S.A. Klein, and G.F. Nellis. 2008. “Experimental Investigation of the Performance of Industrial Evaporator Coils Operating under Frosting Conditions.” *International Journal of Refrigeration* 31(1): 98–106. https://linkinghub.elsevier.com/retrieve/pii/S0140700707001065 (February 19, 2019).

Badri, Deyae, Cyril Toublanc, Olivier Rouaud, and Michel Havet. 2021. “Review on Frosting, Defrosting and Frost Management Techniques in Industrial Food Freezers.” *Renewable and Sustainable Energy Reviews* 151: 111545.

Bockholt, M. et al. 2008. “Transient Modelling of a Controllable Low Pressure Accumulator in CO2 Refrigeration Cycles.” *undefined*.

Fritzson, Peter. 2012. *Introduction to Object-Oriented Modeling and Simulation with Modelica Using OpenModelica*. http://www.modelica (September 16, 2021).

Haaf, Siegfried. 1988. “Wärmeübertragung in Luftkühlern.” In *Wärmeaustauscher*, Springer Berlin Heidelberg, 435–91.

Kim, Donghee, Chiwon Kim, and Kwan Soo Lee. 2015. “Frosting Model for Predicting Macroscopic and Local Frost Behaviors on a Cold Plate.” *International Journal of Heat and Mass Transfer* 82: 135–42. http://dx.doi.org/10.1016/j.ijheatmasstransfer.2014.11.048 (April 22, 2021).

Lemmon, Eric W, Ian H Bell, Marcia L Huber, and Mark O Mclinden. 2021. *REFPROP Documentation Release 10.0*.

Léoni, Aurélia et al. 2016. “State-of-the-Art Review of Frost Deposition on Flat Surfaces.” *International Journal of Refrigeration* 68: 198–217. http://dx.doi.org/10.1016/j.ijrefrig.2016.04.004.

Liu, Jinghui, Qinggang Li, Fazhong Wang, and Lei Zhou. 2012. “A New Model of Screw Compressor for Refrigeration System Simulation.” In *International Journal of Refrigeration*, Elsevier, 861–70.

Mao, Y, Hong Chen, and Robert W. Besant. 1999. “Frost Characteristics and Heat Transfer on a Flat Plate under Freezer Operating Conditions: Part I, Experimentation and Correlations.” *ASHRAE Transactions* 105.

Qiao, Hongtao, and Reinhard Radermacher. 2014. *Transient Modeling of Two-Stage and Variable Refrigerant Flow Vapor Compression Systems with Frosting and Defrosting*.

Richter, Christoph C, and : Braunschweig. *Proposal of New Object-Oriented Equation-Based Model Libraries for Thermodynamic Systems*.

Rouaud, O, and Q T Pham. 2012. “Heat and Mass Transfer Modelling during Freezing of Foodstuffs.” *the 2012 COMSOL Conference* (July).

Schmidt, Roland. 2003. *Eine Methode Zur Numerischen Untersuchung von Strömung Und Wärmeübertragung in Komplexen Geometrien*. Ibidem-Verl.

Shah, R K, and A L London. 1978. *Laminar Flow Forced Convection in Ducts - 1st Edition*. 1st Edition. https://www.elsevier.com/books/laminar-flow-forced-convection-in-ducts/shah/978-0-12-020051-1 (December 1, 2021).

Strupp, Nils-Christian, Nicholas Lemke, Wilhelm Tegethoff, and Jürgen Köhler. 2007. "Investigation of Low Pressure Accumulators in CO2 Refrigeration Cycles." In *ICR 2007. Refrigeration Creates the Future. Proceedings of the 22nd IIR International Congress of Refrigeration.*, https://iifiir.org/en/fridoc/investigation-of-low-pressure-accumulators-in-co2-refrigeration-cycles-24717 (September 16, 2021).

Tegethoff, Wilhelm. 1999. *Eine Objektorientierte Simulationsplattform Für Kälte-, Klima- Und Wärmepumpensysteme*. VDI-Verl.

VDI Heat Atlas. 2010. VDI Heat Atlas Springer Berlin Heidelberg.

Westhäuser, Jochen et al. 2018. "Untersuchung Der Vereisung von Mikrokanal-Wärmeübertragern."

Wetter, Michael, Wangda Zuo, Thierry S. Nouidui, and Xiufeng Pang. 2014. "Modelica Buildings Library." *Journal of Building Performance Simulation* 7(4): 253–70. https://www.tandfonline.com/doi/abs/10.1080/19401493.2013.765506 (May 4, 2021).